AGU PUBLICATIONS

Geochemistry, Geophysics, Geosystems

RESEARCH ARTICLE

10.1002/2015GC006089

Special Section:
Magnetism From Atomic to Planetary Scales: Physical Principles and Interdisciplinary Applications in Geo- and Planetary Sciences

Key Points:
- Magnetic properties of sediments on the source to sink pathway of the Red River are studied
- Magnetic grain-size and mineralogy indicators are sensitive to sediment sorting
- Magnetic proxies of environmental change are more reliable when used with geochemical indicators

Correspondence to:
W. Zhang,
wgzhang@sklec.ecnu.edu.cn

Citation:
Nguyen, T. T. H., W. Zhang, Z. Li, J. Li, C. Ge, J. Liu, X. Bai, H. Feng, and L. Yu (2016), Magnetic properties of sediments of the Red River: Effect of sorting on the source-to-sink pathway and its implications for environmental reconstruction, *Geochem. Geophys. Geosyst.*, *17*, 270–281, doi:10.1002/2015GC006089.

Received 9 SEP 2015
Accepted 28 DEC 2015
Accepted article online 2 JAN 2016
Published online 2 FEB 2016

Magnetic properties of sediments of the Red River: Effect of sorting on the source-to-sink pathway and its implications for environmental reconstruction

Thi Thu Hien Nguyen[1,2], Weiguo Zhang[1], Zhen Li[3], Jie Li[4], Can Ge[1], Jinyan Liu[1], Xuexin Bai[1], Huan Feng[5], and Lizhong Yu[1]

[1]State Key Laboratory of Estuarine and Coastal Research, East China Normal University, Shanghai, China, [2]Institute of Geography, Vietnam Academy of Science and Technology, Hanoi, Vietnam, [3]School of Earth and Ocean Sciences, University of Victoria, Victoria, British Columbia, Canada, [4]Yunnan Institute of Environmental Science, Kunming, China, [5]Department of Earth and Environmental Studies, Montclair State University, Montclair, New Jersey, USA

Abstract We conducted a mineral magnetic study of river bank and subaqueous delta sediments from the Red River, in order to examine the role of sedimentary sorting on the variation of sedimentary magnetic properties from source to sink. The magnetic mineralogy mainly consists of magnetite and hematite. Bulk sediment particle-size variations have a strong influence on magnetic properties, with the frequently used magnetic parameters χ_{fd}%, χ_{ARM}, χ_{ARM}/χ, and χ_{ARM}/SIRM exhibiting positive correlations with the <4 μm fraction, while S-ratios are negatively correlated with this fraction. Compared with river bank sediments and shallow shoreface (<5 m water depth) sediments, sediments from the deeper (>5 m water depth) part of the subaqueous delta have lower χ and SIRM values, a finer ferrimagnetic grain-size and higher proportions of hematite, consistent with selective loss of coarse ferrimagnetic grains on the source-to-sink pathway. We suggest that variations in magnetic properties in response to particle-size compositions and therefore depositional environment changes should be carefully addressed when magnetic proxies such as χ_{ARM}/SIRM are used in the study of coastal and marine environmental changes (e.g., sea-level change). In such cases, the combined use of magnetic properties and geochemical indicators, such as Al/Ti ratio, may provide better results for paleoenvironmental reconstruction.

1. Introduction

The large rivers in Asia deliver huge amounts of sediment to the global ocean [*Milliman and Meade*, 1983]. The accumulations of these sediments in deltas and continental margins contain valuable information about geological history, climate changes, and human activity in the river catchment and thus they have been extensively studied to reconstruct environmental changes on different time scales [e.g., *Colin et al*., 1998; *Kissel et al*., 2003; *Bianchi and Allison*, 2009; *Wan et al*., 2015]. Geochemical and mineralogical methods are conventionally used to characterize sediments derived from these large rivers [e.g., *Clift et al*., 2008; *Wan et al*., 2015]. A number of indicators have been developed [e.g., *Clift et al*., 2014, and references therein], such as the conservative Al/Ti ratio for sediment provenance [*Young and Nesbitt*, 1998], and the chemical index of alteration (CIA) [*Nesbitt and Young*, 1982] for climate changes. In addition to geochemical and mineralogical methods, magnetic properties of sediments have been increasingly used as a climate proxy, provenance tracer, and ocean productivity indicator [e.g., *Colin et al*., 1998; *Kissel et al*., 2003; *Larrasoana et al*., 2003; *Li et al*., 2006a; *Suganuma et al*., 2009]. Magnetic grain-size parameters (e.g., χ_{ARM}/SIRM) have been commonly used to indicate glacial-interglacial-scale climate change or sea-level change [*Colin et al*., 1998; *Kissel et al*., 2003; *Ouyang et al*., 2014]. Before these parameters can be used as a reliable "proxy" or indicator, the factors influencing sediment transfer processes, and thus indirectly the proxies themselves, must be thoroughly understood. This is demonstrated by the effect of sedimentary sorting on Al/Ti ratios and other proxies [*Shao et al*., 2012; *Chen et al*., 2013], which may result in the variations of these indices reflecting factors other than direct provenance or climate change. Therefore, these coupled fluvial-marine systems have been increasingly investigated in source-to-sink studies [e.g., *Liu et al*., 2007; *Bianchi and Allison*, 2009; *Wan et al*., 2015].

Sediments in the delta region and the margin of the South China Sea have been extensively studied to reconstruct the history of local delta formation, the evolution of the South China Sea, and their relationships with the Asian monsoon and tectonic uplift of the Tibetan Plateau [*Li et al*., 2006b; *Wan et al*., 2015]. In particular, several studies have investigated the magnetic properties of sediments from the South China Sea in order to reconstruct paleoenvironmental changes [*Kissel et al*., 2003; *Ouyang et al*., 2014; *Wang et al*., 2014]. However, a source-to-sink analysis of sediments delivered to the South China Sea using a magnetic approach has not yet been reported but is clearly important for the development of magnetic-based paleoenvironmental proxies. Several studies have demonstrated that magnetic properties of sediments are sensitive to bulk sediment particle-size, which is strongly influenced by hydrodynamics [*Oldfield et al*., 1985; *Zhang and Yu*, 2003; *Oldfield et al*., 2009; *Hatfield and Maher*, 2009; *Liu et al*., 2010]. Therefore, sediments from the same source may have different magnetic properties due to sediment sorting along the pathway of the sediment routing system. The Red River is one of the large rivers originating from the Tibetan Plateau, with a historically high sediment load of 160 Mt/yr discharged into the South China Sea [*Milliman and Meade*, 1983]. Recently, the sediment flux drastically decreases to approximately 40 Mt/yr during the 1997–2004 period following the Hoa Binh Dam impoundment [*Le et al*., 2007; *Vinh et al*., 2014]. In the present research, we studied the magnetic properties, together with the Al/Ti ratios, of the Red River sediments along the transfer pathway from land to sea, in order to understand the influence of bulk sediment particle-size and hence depositional environment on the propagation of the magnetic signal from source-to-sink.

2. Study Area

The Red River originates from the mountainous area in the Yunnan province of China, flows 1200 km southeastward and then flows through seven Vietnamese provinces before entering the South China Sea. The Red River in Vietnam has two major tributaries: The Da River and Lo River, with their head sources in China (Figure 1). The catchment of the Red River is dominated by Paleozoic sedimentary rocks with metamorphic and igneous rocks also present, mainly along the main channel and in the Lo subbasin [*Borges and Huh*, 2007]. The river basin is within a subtropical monsoon climate region with a mean annual rainfall of about 1590 mm. The wet season (from May to October) accounts for 85–95% of the total annual rainfall. Mean annual temperature in the upstream region ranges from 14–16°C in winter to 26–27°C in summer, while in the delta area the temperature is higher, ranging from 17 to 30°C [*Le et al*., 2007].

The average total discharge of the Red River into the sea is 3500 m^3/s (1960–2008) [*Dang et al*., 2010]. The mountainous areas that form a large part of the upstream basin of the Red River are tectonically very active and have high erosion rates [*Le et al*., 2007]. Most of the sediments come from the main stream of Red River (called the Thao River), with a subordinate contribution from the Lo river, and minor contribution from the Da river after the closure of the Hoa Binh dam in 1989 (Figure 1). According to the Food and Agriculture Organization classification system, soils in the upper basin are typically Acrisols and Ferrasols [*Gong*, 1999], and the red color of the eroded laterite soils is responsible for the name of the river.

At present, 37.8% of the fluvial sediment is discharged through the Ba Lat mouth, 23.7% through the Day river mouth, 11.8% through the Tra Ly River mouth, and 11.7% through the Van Uc and Thai Binh river mouths (Figure 1) [*Duc et al*., 2007]. The coast adjacent to the Ba Lat has a diurnal tidal regime with average amplitude of 2.5–3.5 m. Due to the monsoon climate, the waves approach the coast from the northeast in winter and from the south in summer. The average and maximum wave heights are 0.7–1.3 m and 3.5–4.5 m, respectively [*Duc et al*., 2007]. Geomorphologically, the subaqueous delta can be divided into an erosional shoreface zone (water depth $<$5 m), a delta front at the Ba Lat mouth, and a prodelta zone (5–30 m) [*van den Bergh et al*., 2007]. Sand is dominant in the shoreface zone due to the stronger hydrodynamics, and silts are dominant in the delta front and clayey silts in the prodelta zone [*Duc et al*., 2007].

3. Samples and Methods

Most of the sediment samples were collected as part of a larger sampling program conducted in the Red River catchment in 2007, with additional samples collected in 2014. In total, 26 surface sediment samples were obtained from the river bank along the main channel and 18 subaqueous sediment samples from the delta (Figure 1). All of the samples were dried at 40°C and then disaggregated prior to analysis.

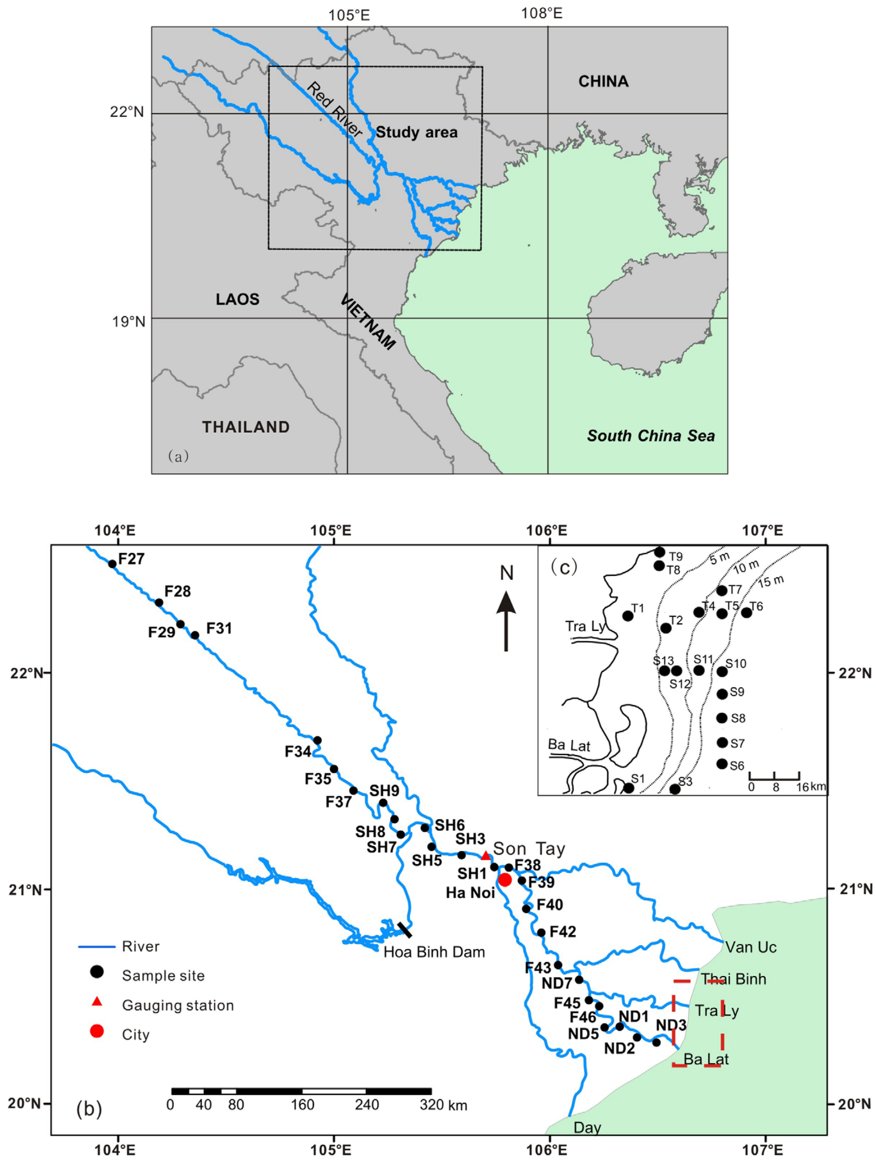

Figure 1. (a) Map of the study area, with the sampling sites detailed in Figure 1b. The red rectangle in Figure 1b indicates the (c) inset map, in which the sampling sites in the subaqueous delta are shown.

Particle-size distribution was measured using a laser-diffraction analyzer (Coulter LS-100Q) following pretreatment with 0.2 M HCl and 5% H_2O_2 to remove biogenic carbonate and organic matter, respectively. Sodium hexametaphosphate (0.5 M $(NaPO_3)_6$) was added to ensure complete disaggregation prior to analysis [*Ru*, 2000].

Low-frequency (0.47 kHz) and high-frequency (4.7 kHz) magnetic susceptibility (χ_{lf} and χ_{hf}, respectively) were measured using a Bartington magnetic susceptibility meter and MS2B dual-frequency sensor. Frequency-dependent susceptibility (χ_{fd}%) was calculated as $\chi_{fd}\% = (\chi_{lf} - \chi_{hf})/\chi_{lf} \times 100$. Anhysteretic remanent magnetization (ARM) was imparted in a 0.04 mT direct current field superimposed on a peak AF demagnetization field of 100 mT, and is expressed as susceptibility of ARM (χ_{ARM}). Isothermal remanent magnetization (IRM) was first imparted at 2 T and then at backfields of -100 mT and -300 mT. These remanences are referred to as SIRM, IRM_{-100mT}, and IRM_{-300mT}, respectively, and are mass normalized. Hard isothermal remanent magnetization (HIRM) was defined as $HIRM = (SIRM + IRM_{-300mT})/2$. S_{-100} and S_{-300} were calculated as $S_{-100} = 100 \times (SIRM - IRM_{-100mT})/(2 \times SIRM)$ and $S_{-300} = 100 \times (SIRM - IRM_{-300mT})/(2 \times SIRM)$, respectively. By this definition, S_{-100} and S_{-300} vary from 0% to 100%.

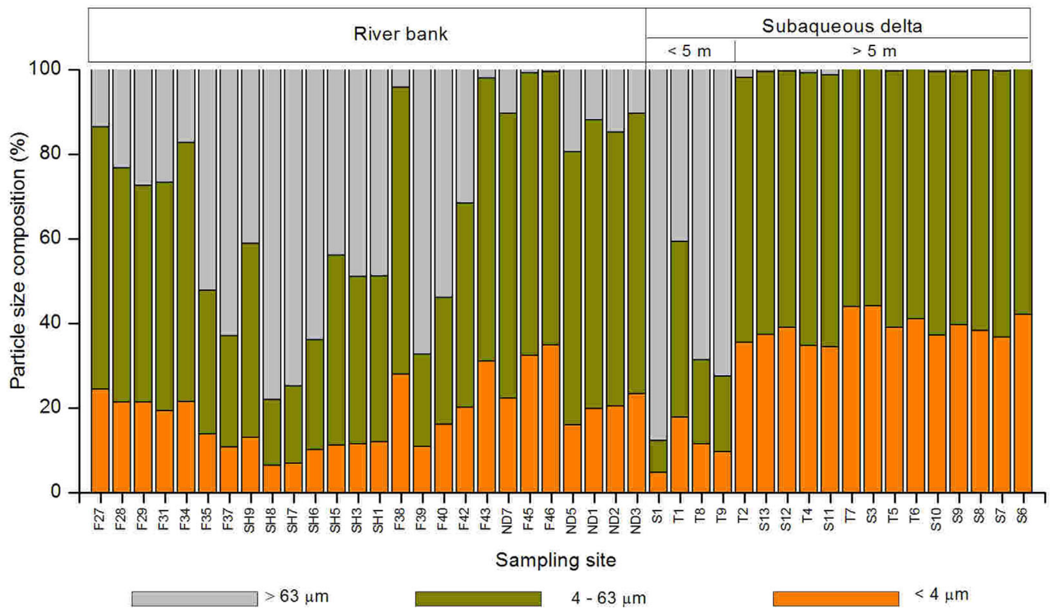

Figure 2. Spatial variation of particle-size composition of the river bank and subaqueous sediments. The fluvial samples are arranged in an order from upstream down to the coast. The subaqueous delta samples are grouped into shoreface (water depth <5 m) and prodelta (water depth >5 m) zones. Clearly, sediments from the prodelta zones have the highest clay fraction on average.

IRM acquisition curves on selected samples were measured in 39 fields using an MMPM10 pulse magnetizer. The IRM acquisition curves were unmixed using the method of *Kruiver et al*. [2001]. Measurements of the temperature-dependent magnetic susceptibility were made using an AGICO MFK1-FA Kappabridge equipped with a CS-3 high-temperature furnace. Each sample was heated from room temperature to 700°C and then cooled to room temperature in an argon atmosphere.

Magnetic minerals from selected samples were extracted following method described in *Walden et al*. [1999], and were analyzed by X-ray diffraction (XRD) using a Philips PW 1710 diffractometer with CuKα radiation (40 mA, 40 kV). The measurements were performed using a step size of 0.02° in the 2θ range from 5° to 80°.

The concentrations of Al and Ti in the bulk samples were determined using inductively coupled plasma atomic emission spectrometry (iCAP™ 7400 ICP-OES Analyzer) after a mixed HF-HNO_3-$HClO_4$ digestion [*National Environmental Bureau* (*NEB*), 1998]. The China national reference material GSD9 was included for quality control. The analytical precision and error of the analysis are within 10%.

4. Results

4.1. Particle-Size Distributions

The spatial variation of particle-size composition is shown in Figure 2, with sampling sites arranged in order from upstream to the coast. In general, from upstream down to the river mouth (sites F27 to ND3), the sediments initially become coarser and then finer. The coarsest sediments occur between sites F35 and F42, with the sand fraction (>63 μm) comprising 52%. The sites downstream of F42 are dominated by the silt fraction (4–63 μm). In the subaqueous delta, sediments from the shoreface (water depth <5 m, comprising sites S1, T1, T8, and T9) are dominated by the sand fraction. Sediments from greater water depths are dominated by silts and clays (<4 μm) with a negligible sand fraction. This spatial pattern of sediment texture variation is in accordance with previous findings [*Duc et al*., 2007; *van den Bergh et al*., 2007]. On average, the prodelta sediments have a higher clay fraction than the river bank sediments (Figure 2).

4.2. Magnetic Properties

Magnetic susceptibility (χ) and SIRM generally reflect the concentration of magnetic minerals. Unlike χ, SIRM is not influenced by (super)paramagnetic and diamagnetic minerals [*Thompson and Oldfield*, 1986]. χ

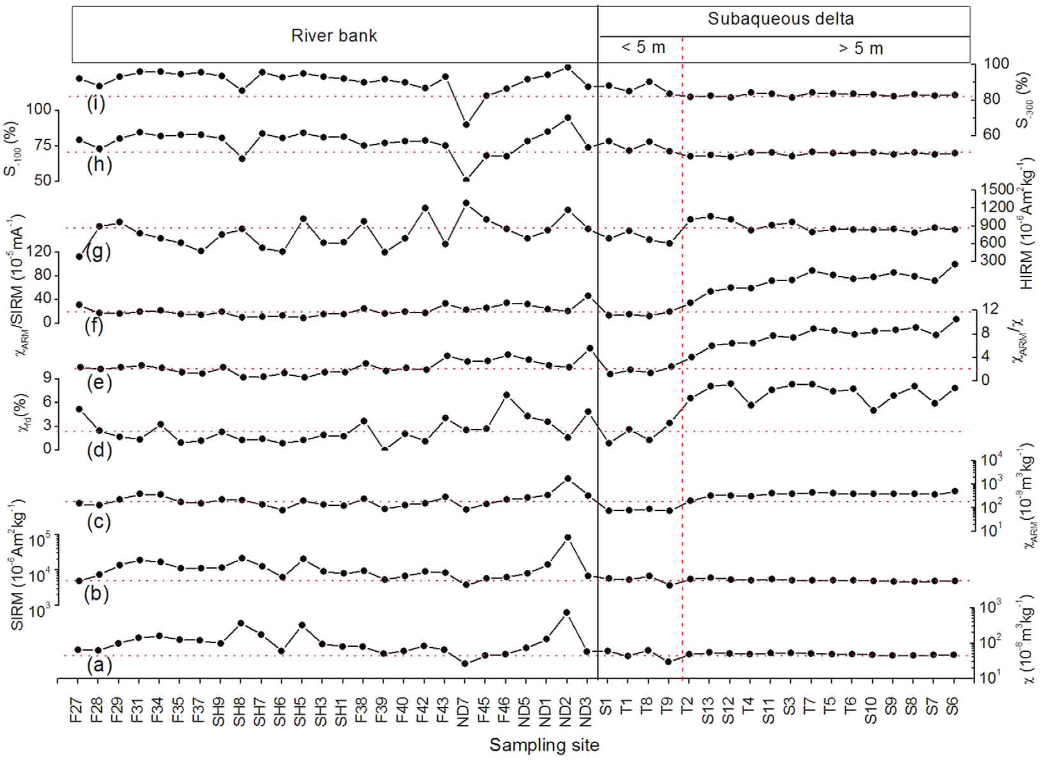

Figure 3. Spatial variation of magnetic properties of the river bank and subaqueous sediments. The fluvial samples are arranged in order from upstream down to the coast. The subaqueous delta samples are grouped into shoreface (water depth <5 m) and prodelta (water depth >5 m) zones. The red lines depict the mean values either for the (d–f) river bank or the (a–c and g–i) prodelta sediments. (a and b) The river bank sediments have relatively high χ and SIRM values, suggesting higher ferrimagnetic mineral concentrations. Sediments from the prodelta have higher χ_{fd}%, χ_{ARM}/χ, χ_{ARM}/SIRM values (Figures 3d–3f), which suggests that the ferrimagnetic minerals become finer in the prodelta sediments.

and SIRM exhibit a similar pattern of spatial variation, suggesting that χ is dominated by ferrimagnetic minerals (Figures 3a and 3b). The river bank sediments exhibit fluctuating χ and SIRM values, while the subaqueous delta sediments have more uniform values, indicating that ferrimagnetic mineral concentrations in the former are more variable. On average, the river bank sediments have higher χ and SIRM values, suggesting higher ferrimagnetic mineral concentrations. χ_{ARM} is sensitive to stable single domain (SD, 0.04–0.06 μm) ferrimagnetic grains [Maher, 1988] and in comparison with χ and SIRM the difference in χ_{ARM} values between the river bank and subaqueous delta samples is less significant (Figure 3c).

χ_{fd}% is an estimation of the relative contribution of fine, viscous superparamagnetic (SP, $\sim<$0.03 μm for magnetite) grains to the total magnetic assemblage [*Thompson and Oldfield*, 1986]. The ratio χ_{ARM}/χ can be used to indicate the grain-size of magnetic minerals, with higher values reflecting fine grained SD grains and lower values multidomain (MD) or SP grains [Maher, 1988]. The ratio χ_{ARM}/SIRM is also indicative of grain-size, but it is unaffected by SP particles and therefore lower values correspond to coarser MD grains. These three parameters generally exhibit similar spatial trends, i.e., they are relatively stable from upstream down to the river mouth, and then increase significantly from the shoreface zone to the prodelta with increasing water depth (Figures 3d–3f). The subaqueous prodelta sediments have much higher values than their fluvial counterparts. This suggests that the ferrimagnetic minerals become finer-grained with increases in the clay and silt fractions and decreases in the sand fraction.

HIRM is commonly used to estimate the abundance of imperfect antiferromagnetic minerals such as goethite and hematite [*Bloemendal and Liu*, 2005]. Here it exhibits no clear trend along the sediment transport pathway (Figure 3g). S_{-300} is a measure of the relative importance of low-coercivity (e.g., magnetite and maghemite) and high-coercivity components in the total magnetic mineral assemblage [*Bloemendal and Liu*, 2005], while S_{-100} reflects the ratio of low-coercivity minerals to medium-coercivity and high-coercivity minerals [*Yamazaki*, 2009; *Yamazaki and Ikehara*, 2012]. Both parameters are higher in the river bank

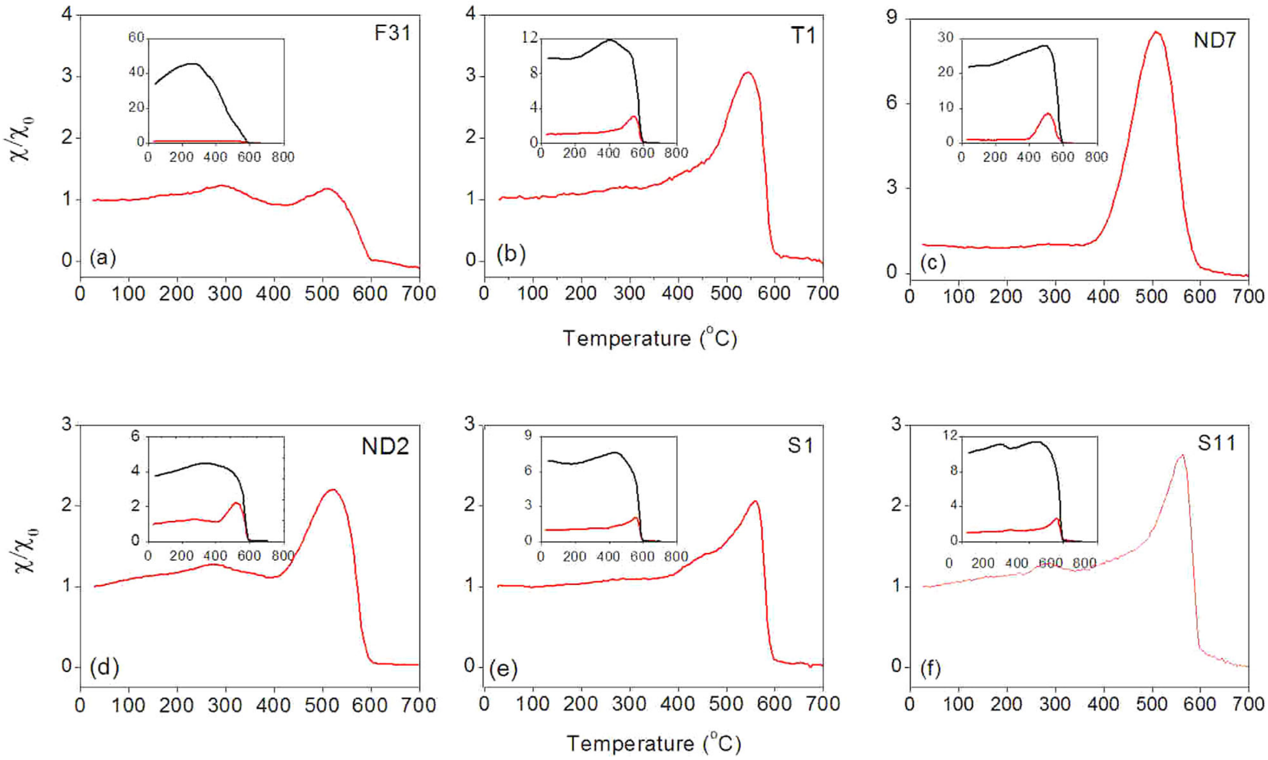

Figure 4. Magnetic susceptibility changes during heating from room temperature to 700°C. The complete cycle of χ versus temperature measurement is shown in the insets. Red and blue lines represent heating and cooling curves, respectively. All the samples have T_c around 580°C which is typical of magnetite. (a, c, and f) Some samples show a decreases of χ with increasing temperature beyond 580°C, which is probably due to the presence of hematite.

sediments and lower in the subaqueous delta sediments, suggesting higher proportions of ferrimagnetic minerals in the former (Figures 3h and 3i).

In all samples, the susceptibility versus temperature (χ-T) analysis reveals a Curie temperature of 580°C, which is indicative of magnetite [*Thompson and Oldfield*, 1986] (Figure 4). Some of the samples exhibit an increase of χ before peaking at about 300°C (Figures 4a and 4d), which may result from the gradual unblocking of fine-grained ferrimagnetic particles [*Liu et al*., 2005]. All of the curves exhibit notable peaks at about 510°C, which may be the result of the conversion of iron-containing silicates to magnetite [*Liu et al*., 2005]. Some of the samples exhibit a continuous decrease in χ after heating above 580°C, which is probably due to the presence of hematite (Figures 4a, 4c, and 4f).

Typical IRM acquisition curves are illustrated in Figure 5. The IRM acquisition curves can be described by two dominant components, with median fields $B_{1/2}$ of ~38 and ~700 mT, which probably correspond to magnetite and hematite, respectively [*Kruiver et al*., 2001; *Yamazaki and Ikehara*, 2012]. This is in accordance with the thermomagnetic results (Figure 4). XRD analysis also confirms the presence of magnetite and hematite (Figure 6). Some of the samples have an additional high-coercivity component of ~2000 mT, which is typical of goethite [*Kruiver et al*., 2001]. In general, the ~38 mT coercivity component is the dominant contributor to the IRM, but in some samples the high-coercivity hematite component has a stronger contribution (Figure 5b).

4.3. Relationship Between Bulk Sediment Particle-Size and Magnetic Properties

Correlation analysis reveals diverse relationships between bulk sediment particle-size and magnetic properties (Table 1). Concentration-related parameters (χ, SIRM, HIRM) are not significantly correlated with particle-size. χ_{ARM} exhibits weak relationships with the silt and sand fractions. However, if one sample with an extremely high χ_{ARM} value (ND2) is removed, then χ_{ARM} is also significantly correlated with the clay fraction ($R^2 = 0.60$) (Figure 7a). Magnetic grain-size, reflected by χ_{ARM}/χ, χ_{ARM}/SIRM, χ_{fd}%, exhibits a significant positive relationship with the 4–63 and <4 μm fractions, but a negative relationship with the fraction >63 μm (Table 1 and Figures 7d–7f). The positive relationship between χ_{ARM}/χ, χ_{ARM}/SIRM, and the clay fraction

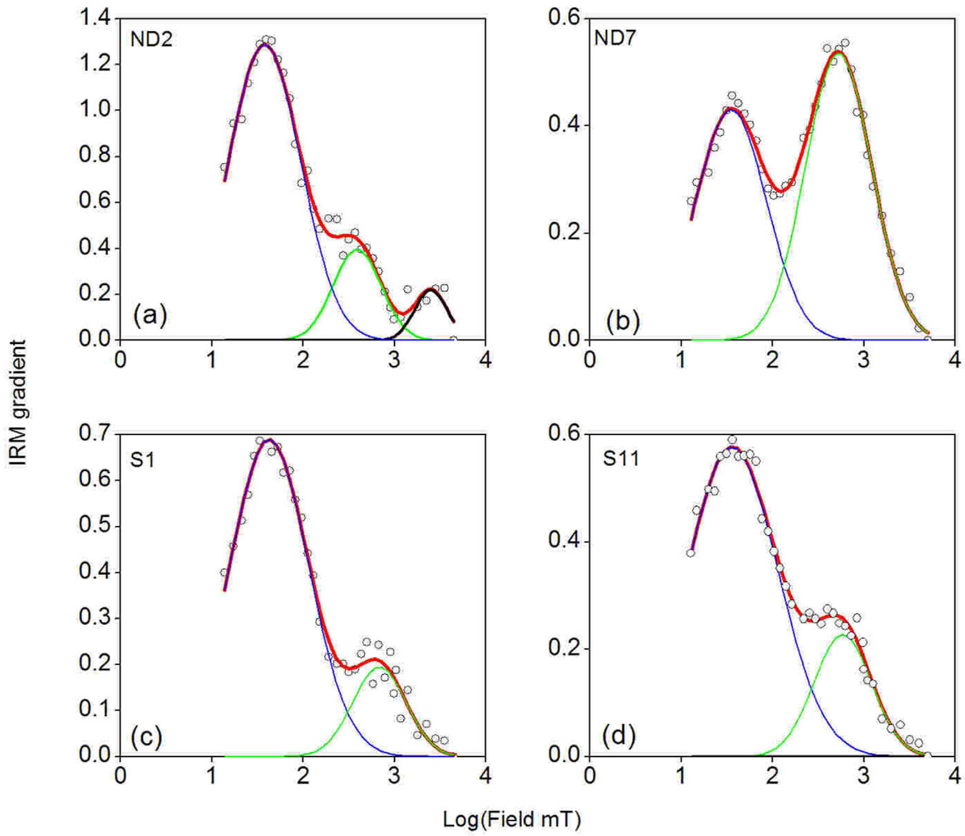

Figure 5. Results of isothermal remanent magnetization (IRM) unmixing analysis [*Kruiver et al.*, 2001] for selected samples. Two dominant components are identified, with the lower-coercivity and higher-coercivity component ($B_{1/2}$ around 38 mT and 700 mT) corresponding to magnetite and hematite, respectively.

is different for the river bank ($R^2 = 0.60$ and 0.52, respectively) and subaqueous delta deposits ($R^2 = 0.19$ and 0.28, respectively), with the regression line for the latter displaying a gentler slope (Figures 7d and 7e). In contrast S-ratios are positively correlated with the sand fraction but negatively correlated with the finer fractions (Table 1 and Figures 7b, 7c). It is also clear that the shallower subaqueous delta sediments have a different S-ratio versus clay fraction relationship from that of the river bank and deeper prodelta delta sediments (Figures 7b and 7c).

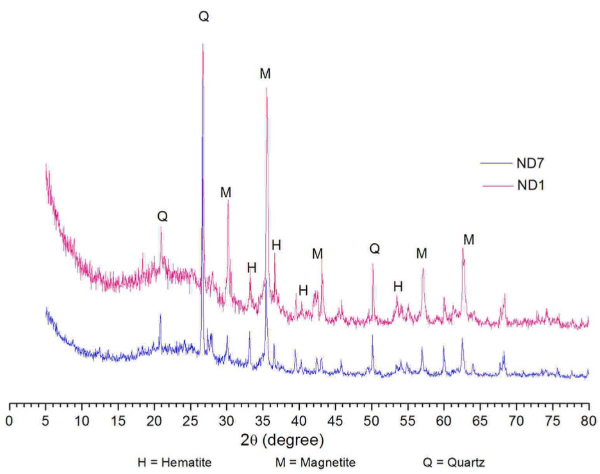

Figure 6. XRD spectra for extracted magnetic minerals, demonstrating the presence of both magnetite (M) and hematite (H).

5. Discussion

5.1. Magnetic Mineralogy and the Influence of Bulk Sediment Particle-Size on Magnetic Properties

Magnetic and XRD analyses reveal that magnetite is the dominant ferrimagnetic mineral in the sediments in terms of contribution to the bulk magnetic properties. Hematite, an imperfect antiferromagnetic mineral, is also well-represented magnetically. This agrees well with the dominant soil types found in the study area: due to the subtropical climate and strong

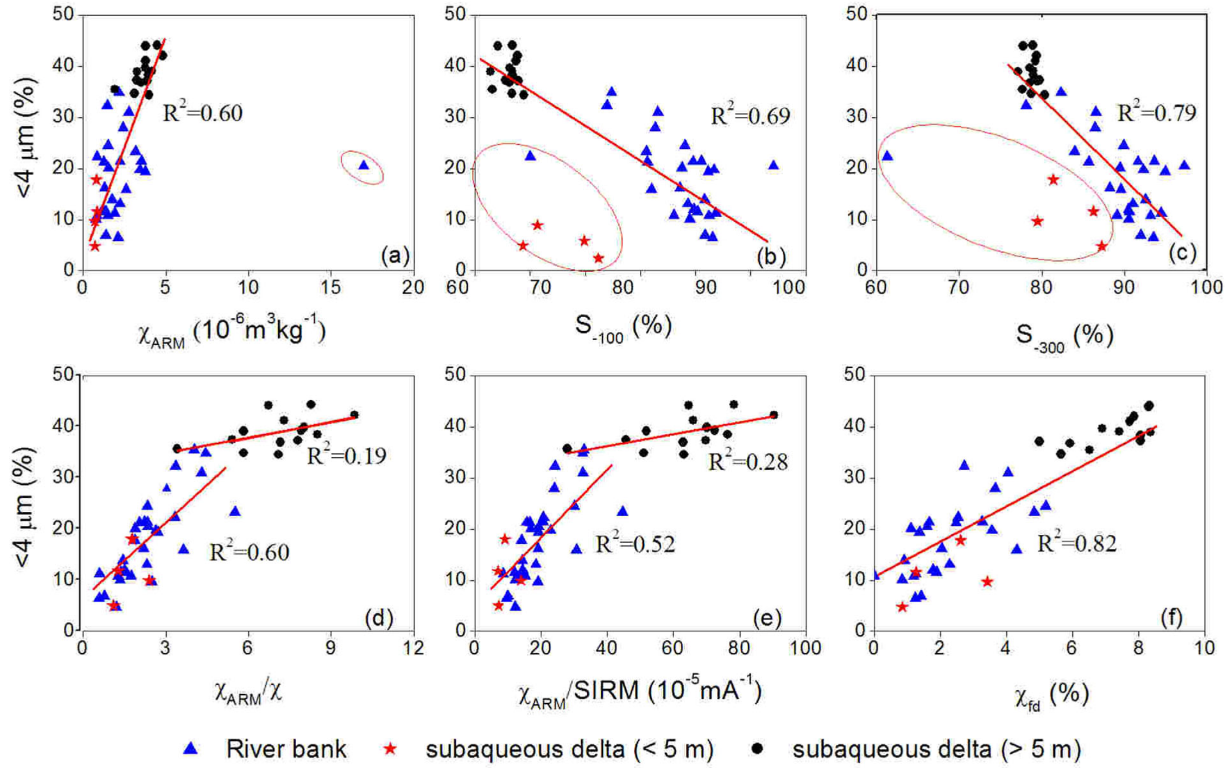

Figure 7. Scatter plot of clay fraction (<4 μm) percentage versus magnetic parameters (a) χ_{ARM}, (b) S_{-100}, (c) S_{-300}, (d) χ_{ARM}/χ, (e) χ_{ARM}/SIRM, and (f) χ_{fd}%. The subaqueous delta samples are grouped into shoreface (water depth <5 m) and prodelta (water depth >5 m) zones. In Figures 7a–7c, the correlation coefficients are calculated without the samples in circles. (a and d–f) The positive relationships between χ_{ARM}, χ_{ARM}/χ, χ_{ARM}/SIRM, χ_{fd}%, and the <4 µm fractions suggest the association of fine-grained ferrimagnetic minerals with the clay factions. (b and c) The negative relationships between S-ratios and the clay fractions suggest that higher proportions of antiferromagnetic minerals in the clay fraction. (d and e) χ_{ARM}/χ and χ_{ARM}/SIRM show stronger relationships with the clay fraction in the river bank sediments than those in the prodelta sediments.

chemical weathering, Acrisols and Ferrasols are the dominant soil type in the upstream section part of Red River, which has a red color due to the presence of hematite pigment [*Gong*, 1999].

In fluvial and coastal environments, hydrodynamic variations can result in particle-size and mineralogical sorting during the course of sediment transport and deposition [*D'Haen et al.*, 2012; *Rahman and Plater*, 2014]. Bulk sediment particle-size variations can have an important effect on magnetic properties, even if the sediment source does not vary [*Oldfield et al.*, 1985; *Oldfield and Yu*, 1994; *Zhang and Yu*, 2003]. In the present study, the significant correlations between χ_{fd}%, χ_{ARM}, and the clay fraction suggest that fine-grained SP/SD ferrimagnetic grains are concentrated within this fraction. Although the relationships between χ and SIRM and particle-size are not significant, it seems that these two parameters tend to reflect the presence of coarse-grained ferrimagnetic minerals associated with the sand fraction (Table 1). Since soil weathering in tropical/subtropical areas can produce fine-grained secondary ferrimagnetic minerals [*Lu et al.*, 2015], we suggest that the SD/SP grains are of pedogenic origin, while the coarse MD grains are of detrital origin.

χ_{fd}%, χ_{ARM}/χ, and χ_{ARM}/SIRM are generally stable from upstream down to site F39, and then increase slightly toward the river mouth. In the subaqueous delta, they show increasing trends from shallow water to deeper water, suggest a fining of the ferrimagnetic grain-size with distance away from the coast, with larger grains

Table 1. Correlation Coefficients Between Magnetic Properties, Al/Ti Ratio and Particle-Size ($n = 44$)[a]

	χ	SIRM	χ_{fd}%	HIRM	χ_{ARM}	χ_{ARM}/χ	χ_{ARM}/SIRM	S_{-100}	S_{-300}	Al/Ti
<4 µm	−0.31	−0.22	**0.84**	0.27	0.33	**0.90**	**0.88**	**−0.67**	**−0.65**	**0.81**
4–63 µm	−0.08	0.04	**0.59**	**0.44**	**0.41**	**0.58**	**0.53**	**−0.42**	−0.39	**0.58**
>63 µm	0.18	0.07	**−0.74**	−0.39	**−0.40**	**−0.76**	**−0.72**	**0.56**	**0.53**	**−0.71**

[a]Bold type indicates significance at $p < 0.01$.

deposited first and finer grains carried further seaward (Figure 3). The slight increase of these parameters starts at site F39, where the Red River branches into a number of distributaries. This trend is consistent with the decrease in fluvial energy when approaching the river mouth; however, the trend is reversed in the coastal shoreface zone where the water depth is shallower than 5 m. Here the sediments are dominated by sands due to strong wave activity and resultant winnowing of the finer particle-size fractions. In deeper water, in the prodelta environments, the sediments are the finest and $\chi_{fd}\%$, χ_{ARM}/χ, and χ_{ARM}/SIRM reach their highest values. A similar fining trend of ferrimagnetic minerals has been observed in the suspended sediments and floodplain sediments of the Yangtze River [*Li et al*., 2012], as well as in the suspended estuarine sediments of the Yangtze Estuary [*Dong et al*., 2014].

As a result, χ_{ARM}/χ, χ_{ARM}/SIRM, $\chi_{fd}\%$ are positively correlated with the clay fraction and to a lesser degree, the silt fraction (Table 1 and Figures 7d–7f). Although the present study using a laser-based particle-size analysis, which is different from previous ones [e.g., *Oldfield and Yu*, 1994], the relationship is similar to those in the coastal sediments of the Irish Sea [*Oldfield and Yu*, 1994] and the Yangtze Estuary [*Zhang and Yu*, 2003]. It indicates that the use of $\chi_{fd}\%$, χ_{ARM}/χ, and χ_{ARM}/SIRM as proxies for the fine-grained sediment fraction is valid in a number of coastal environments without significant postdepositional diagenetic dissolution [e.g., *Dessai et al*., 2009; *Alagarsamy*, 2009].

It is also clear that the subaqueous delta sediments have lower S-ratios (Figure 3). This can be explained by the higher proportions of SD ferrimagnetic minerals as well as pedogenic imperfect antiferromagnetic hematite in the finer sediments. This finding is consistent with the fact that secondary iron oxides formed during soil pedogenesis are generally fine-grained and are enriched in the clay fraction [*Cornell and Schwertmann*, 2003; *Lu et al*., 2015]. It is noteworthy that shoreface sediments have lower S-ratios compared to their river bank counterparts (Figures 7b and 7c). This could be caused by the fact that coarse magnetite grains are preferentially deposited in the river bank zones due to higher density. In spite of the coarser grain-size, the concentration of magnetite in the shoreface sediments is lower. Reductive diagenesis of magnetic minerals in marine environments could also lead to selective dissolution of ferrimagnetic minerals in comparison to antiferromagnetic minerals [e.g., *Robinson et al*., 2000; *Rowan et al*., 2009]. This factor needs to be further studied.

5.2. Implications for Paleoenvironmental Reconstruction

The dependence of magnetic properties on bulk sediment particle-size has been used to infer hydrodynamic variations in fluvial, coastal and estuarine environments [*Hatfield et al*., 2010; *Gallaway et al*., 2012; *Dong et al*., 2014] and the present study confirms these findings. In particular, it has been observed that the magnetic grain-size indicators χ_{ARM}/χ and χ_{ARM}/SIRM, $\chi_{fd}\%$, have a positive relationship with the clay fraction, while S-ratios exhibit the opposite trend with the clay fraction (Figure 7). It is also noteworthy that in the prodelta environment, characterized by fine silt and clay sediments, relatively small changes in the clay fraction have a large effect on the ferrimagnetic grain-size indicators (Figures 7d and 7e). This implies that in sedimentary environments with weak hydrodynamics, ferrimagnetic minerals are especially sensitive to hydrodynamic sorting. In this context, magnetic grain-size indicators have been used as an indicator of the relative distance of the marine coring site to the land, with increasing distance leading to finer bulk sediment particle-sizes and a fining of the ferrimagnetic grain-size distribution [*Wang et al*., 2014]. This relationship has been used to interpret shifts in the coastline during glacial/interglacial periods in response to climate and sea-level changes [*Ouyang et al*., 2014]. Considering the response of S-ratios to particle-size, like magnetic grain-size indicators, S-ratios may be used in a similar way for paleoenvironmental reconstruction. That is a lower S-ratios may indicate a deeper water environment which may be caused by sea level changes. Given the possibility of the dissolution of ferrimagnetic minerals under reducing conditions, the use of a combination of S-ratios and the grain-size indicators ($\chi_{fd}\%$, χ_{ARM}/χ, and χ_{ARM}/SIRM), could be an effective approach, since imperfect antiferromagnetic minerals are more resistant to reductive dissolution compared to ferrimagnetic minerals [*Robinson et al*., 2000; *Rowan et al*., 2009].

In some case, coastal progradation under a stable sea-level will result in changes in sedimentary environments and thus to particle-size variations. For example, in a prograding delta coast, the transition from a prodelta to a delta front at the coring site would lead to a coarsening of the particle-size [*Rahman and Plater*, 2014] and therefore to a lowering of χ_{ARM}/χ and χ_{ARM}/SIRM values upward within a sediment core. In this case, a detailed sedimentary facies analysis would clarify the exact mechanisms responsible for magnetic property variations.

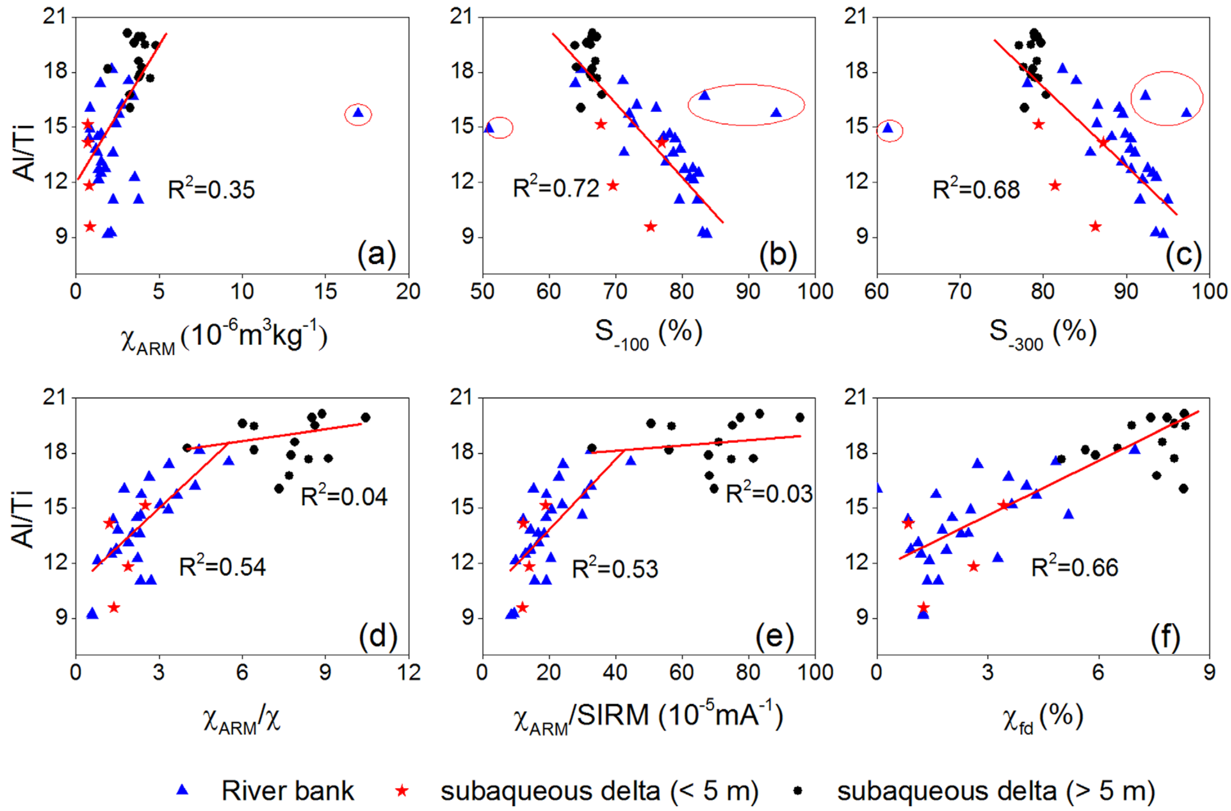

Figure 8. Scatter plot of the Al/Ti ratio versus magnetic parameters (a) χ_{ARM}, (b) S_{-100}, (c) S_{-300}, (d) χ_{ARM}/χ, (e) χ_{ARM}/SIRM, and (f) χ_{fd}%. The subaqueous delta samples are grouped into shoreface (water depth <5 m) and prodelta (water depth > 5 m) zones. In Figures 8a–8c, the correlation coefficients are calculated without the samples in circles. (d and e) Note the different relationships between χ_{ARM}/χ, χ_{ARM}/SIRM, and Al/Ti for the river bank and prodelta sediments. (a and d–f) In general, Al/Ti ratio displays positive relationships with χ_{ARM}, χ_{ARM}/χ, χ_{ARM}/SIRM, and χ_{fd}%, (b and c) while negative relationships with S-ratios.

The Al/Ti ratio has been used for sediment source tracing and the approach is partly based on the conservative behavior of Al and Ti. Given that particle-size influences geochemical composition, it would be expected that Al/Ti would also be influenced by particle-size (Table 1): Ti-containing heavy minerals should be preferentially deposited compared to Al-containing clay minerals thereby increasing the Al/Ti ratio of finer-grained sediments. This effect has been reported in previous studies in which it has been suggested that Al/Ti ratio may be used as a proxy for sea level change in a closed basin, with a lower ratio corresponding to a lower sea-level [*Chen et al*., 2013]. Correlation analysis indicates that S-ratios exhibit negatively relationships with Al/Ti ratio (Figures 8b and 8c), while χ_{ARM} and χ_{fd}% are positively correlated with Al/Ti ratio (Figures 8a and 8f). Magnetic parameters χ_{ARM}/χ and χ_{ARM}/SIRM show similar positive relationship with Al/Ti ratio, except for the poor relationships in the prodelta sediments (Figures 8d and 8e). Such a poor relationship between magnetic parameters and Al/Ti ratio could be due to the sensitivity of magnetic grain-size to sorting in comparison to particle-size as mentioned above. Overall, it suggests that magnetic grain-size and mineralogy indicators and Al/Ti ratio exhibit similar sorting-dependent effects. Considering that magnetic minerals are sensitive to postdepositional alterations, if these magnetic parameters are significantly correlated with Al/Ti ratios, then the use of magnetic parameters as a proxy for sea level change or for coastal retreatment/advancement can be used with more confidence.

6. Conclusions

The magnetic properties of the Red River sediments are mainly contributed by magnetite and hematite. Along a downstream pathway from the delta plain to the subaqueous delta, χ_{fd}%, χ_{ARM}/χ, and χ_{ARM}/SIRM exhibit increasing trends while S-ratios exhibit the opposite trend in response to sorting and variations in bulk sediment particle-size composition in different depositional environments. Correlation analysis indicates that χ_{fd}%, χ_{ARM}, χ_{ARM}/χ, and χ_{ARM}/SIRM are significantly positively correlated with the clay fraction, while S-ratios are negatively correlated with the clay fraction. This suggests that fine SP/SD ferrimagnetic grains and hematite are preferentially associated with the clay fraction, which is linked to pedogenesis in subtropical and temperate environments. Since particle-size distribution of sediment exerts a strong influence on magnetic properties, the commonly used magnetic proxies for sea-level change and other environmental processes should be used with caution in cases where sediment cores from a deltaic/marine environment exhibit significant variations in particle-size. Knowledge of sedimentary facies and depositional environments would clarify the exact mechanisms responsible for magnetic property variations. Considering the changes in depositional environments and possible postdepositional alternation of magnetic minerals, a combined approach using both conservative geochemical indicators such as Al/Ti ratio and magnetic properties may be better for paleoenvironmental reconstruction.

Acknowledgments
The data presented in this paper are available at the Information Center of the State Key Laboratory of Estuarine and Coastal Research, East China Normal University. Qing Yuan (qyuan@sklec.ecnu.edu.cn) can be contacted for access to the data. This study was supported in part by the National Natural Science Foundation of China (41271223), and the State Key Laboratory Special Fund of China (2012KYYW01). We thank Xuan Phong Dang for help in field sampling, and Jan Bloemendal, Christoph Geiss and an anonymous reviewer for their constructive comments and language improvements.

References

Alagarsamy, R. (2009), Environmental magnetism and application in the continental shelf sediments of India, *Mar. Environ. Res.*, *68*(2), 49–58, doi:10.1016/j.marenvres.2009.04.003.

Bianchi, T. S., and M. A. Allison (2009), Large-river delta-front estuaries as natural ''recorders'' of global environmental change, *Proc. Natl. Acad. Sci. U. S. A.*, *106*(20), 8085–8092, doi:10.1073/pnas.0812878106.

Bloemendal, J., and X. Liu (2005), Rock magnetism and geochemistry of two plio-pleistocene Chinese loess-palaeosol sequences—Implications for quantitative palaeoprecipitation reconstruction, *Palaeogeogr. Palaeoclimatol. Palaeoecol.*, *226*(1–2), 149–166, doi:10.1016/j.palaeo.2005.05.008.

Borges, J., and Y. Huh (2007), Petrography and chemistry of the bed sediments of the Red River in China and Vietnam: Provenance and chemical weathering, *Sediment. Geol.*, *194*(3–4), 155–168, doi:10.1016/j.sedgeo.2006.05.029.

Chen, H., et al. (2013), The Ti/Al molar ratio as a new proxy for tracing sediment transportation processes and its application in aeolian events and sea level change in East Asia, *J. Asian Earth Sci.*, *73*, 31–38, doi:10.1016/j.jseaes.2013.04.017.

Clift, P. D., et al. (2008), Holocene erosion of the Lesser Himalaya triggered by intensified summer monsoon, *Geology*, *36*(1), 79–82, doi:10.1130/G24315A.1.

Clift, P. D., S. M. Wan, and J. Blusztajn (2014), Reconstructing chemical weathering, physical erosion and monsoon intensity since 25 Ma in the northern South China Sea: A review of competing proxies, *Chem. Geol.*, *130*, 86–102, doi:0.1016/j.earscirev.2014.01.002.

Colin, C., C. Kissel, D. Blamart, and L. Turpin (1998), Magnetic properties of sediments in the Bay of Bengal and the Andaman Sea: Impact of rapid North Atlantic Ocean climatic events on the strength of the Indian monsoon, *Earth Planet. Sci. Lett.*, *160*(3–4), 623–635, doi:10.1016/S0012-821X(98)00116-2.

Cornell, R. M., and U. Schwertmann (2003), *The Iron Oxides: Structure, Properties, Reactions, Occurrences and Uses*, John Wiley, Weinheim, Germany.

Dang, T. H., A. Coyne, D. Orange, G. Blanc, H. Etcheber, and L. A. Le (2010), Long-term monitoring (1960–2008) of the river-sediment transport in the Red River Watershed (Vietnam): Temporal variability and dam-reservoir impact, *Sci. Total Environ.*, *408*(20), 4654–4664, doi:10.1016/j.scitotenv.2010.07.007.

Dessai, D. V. G., G. N. Nayak, and N. Basavaiah (2009), Grain size, geochemistry, magnetic susceptibility: Proxies in identifying sources and factors controlling distribution of metals in a tropical estuary, India, *Estuarine Coastal Shelf Sci.*, *85*(2), 307–318, doi:10.1016/j.ecss.2009.08.020.

D'Haen, K., G. Verstraeten, and P. Degryse (2012), Fingerprinting historical fluvial sediment fluxes, *Prog. Phys. Geogr.*, *36*(2), 154–186, doi:10.1177/0309133311432581.

Dong, C., W. Zhang, Q. He, Y. Dong, and L. Yu (2014), Magnetic fingerprinting of hydrodynamic variations and channel erosion across the turbidity maximum zone of the Yangtze Estuary, China, *Geomorphology*, *226*, 300–311, doi:10.1016/j.geomorph.2014.08.008.

Duc, D. M., M. T. Nhuan, C. Van Ngoi, T. Nghi, D. M. Tien, T. C. E. van Weering, and G. D. van den Bergh (2007), Sediment distribution and transport at the nearshore zone of the Red River delta, Northern Vietnam, *J. Asian Earth Sci.*, *29*(4), 558–565, doi:10.1016/j.jseaes.2006.03.007.

Gallaway, E., A. S. Trenhaile, M. T. Cioppa, and R. G. Hatfield (2012), Magnetic mineral transport and sorting in the swash-zone: Northern Lake Erie, Canada, *Sedimentology*, *59*(6), 1718–1734, doi:10.1111/j.1365-3091.2012.01323.x.

Gong, Z. T. (1999), *Chinese Soil Taxonomy: Theory, Method and Application* [in Chinese], Science Press, Beijing, China.

Hatfield, R. G., and B. A. Maher (2009), Fingerprinting upland sediment sources: Particle size-specific magnetic linkages between soils, lake sediments and suspended sediments, *Earth Surf. Processes Landforms*, *34*(10), 1359–1373, doi:10.1002/esp.1824.

Hatfield, R. G., M. T. Cioppa, and A. S. Trenhaile (2010), Sediment sorting and beach erosion along a coastal foreland Magnetic measurements in Point Pelee National Park, Ontario, Canada, *Sediment. Geol.*, *231*(3–4), 63–73, doi:10.1016/j.sedgeo.2010.09.007.

Kissel, C., C. Laj, S. Clemens, and P. Solheid (2003), Magnetic signature of environmental changes in the last 1.2 Myr at ODP site 1146, South China Sea, *Mar. Geol.*, *201*(1–3), 119–132, doi:10.1016/S0025-3227(03)00212-3.

Kruiver, P. P., M. J. Dekkers, and D. Heslop (2001), Quantification of magnetic coercivity components by the analysis of acquisition curves of isothermal remanent magnetisation, *Earth Planet. Sci. Lett.*, *189*(3–4), 269–276, doi:10.1016/S0012-821X(01)00367-3.

Larrasoana, J. C., A. P. Roberts, J. S. Stoner, C. Richter, and R. Wehausen (2003), A new proxy for bottom-water ventilation in the eastern Mediterranean based on diagenetically controlled magnetic properties of sapropel-bearing sediments, *Palaeogeogr. Palaeoclimatol. Palaeoecol.*, *190*, 221–242, doi:10.1016/S0031-0182(02)00607-7.

Le, T. P. Q., J. Garnier, B. Gilles, T. Sylvain, and C. V. Minh (2007), The changing flow regime and sediment load of the Red River, Viet Nam, *J. Hydrol.*, *334*(1–2), 199–214, doi:10.1016/j.jhydrol.2006.10.020.

Li, C., S. Y. Yang, and W. G. Zhang (2012), Magnetic properties of sediments from major rivers, aeolian dust, loess soil and desert in China, *J. Asian Earth Sci.*, *45*, 190–200, doi:10.1016/j.jseaes.2011.10.010.

Li, H., S. Zhang, N. Fang, and H. Wang (2006a), Magnetic records of Core MD77-181 in the Bay of Bengal and their paleoenvironmental implications, *Chin. Sci. Bull.*, *51*(15), 1884–1893, doi:10.1007/s11434-006-2057-5.

Li, Z., Y. Saito, E. Matsumoto, Y. J. Wang, S. Haruyama, K. Hori, and L. Q. Doanh (2006b), Palynological record of climate change during the last deglaciation from the Song Hong (Red River) delta, Vietnam, *Palaeogeogr. Palaeoclimatol. Palaeoecol.*, *235*(4), 406–430, doi:10.1016/j.palaeo.2005.11.023.

Liu, Q. S., C. L. Deng, Y. J. Yu, J. Torrent, M. J. Jackson, S. K. Banerjee, and R. X. Zhu (2005), Temperature dependence of magnetic susceptibility in an argon environment: Implications for pedogenesis of Chinese loess/palaeosols, *Geophys. J. Int.*, *161*(1), 102–112, doi:10.1111/j.1365-246X.2005.02564.x.

Liu, S. M., W. G. Zhang, Q. He, D. J. Li, H. Liu, and L. Z. Yu (2010), Magnetic properties of East China Sea shelf sediments off the Yangtze Estuary: Influence of provenance and particle size, *Geomorphology*, *119*(3–4), 212–220, doi:10.1016/j.geomorph.2010.03.027.

Liu, Z. F., C. Colin, H. Wang, K. P. Le, S. Q. Tong, Z. Chen, and A. Trentesaux (2007), Climatic and tectonic controls on weathering in south China and Indochina Peninsula: Clay mineralogical and geochemical investigations from the Pearl, Red, and Mekong drainage basins, *Geochem. Geophys. Geosyst.*, *8*, Q05005, doi:10.1029/2006GC001490.

Lu, S., S. Wang, and Y. Chen (2015), Palaeopedogenesis of red palaeosols in Yunnan Plateau, southwestern China: Pedogenical, geochemical and mineralogical evidences and palaeoenvironmental implication, *Palaeogeogr. Palaeoclimatol. Palaeoecol.*, *420*, 35–48, doi:10.1016/j.palaeo.2014.12.004.

Maher, B. A. (1988), Magnetic properties of some synthetic sub-micron magnetites, *Geophys. J.*, *94*(1), 83–96, doi:10.1111/j.1365-246X.1988.tb03429.x.

Milliman, J. D., and R. H. Meade (1983), World-wide delivery of river sediment to the oceans, *J. Geol.*, *91*(1), 1–21, doi:10.1086/628741.

National Environmental Bureau (NEB) (1998), *Water and Waste Water Analysis* [in Chinese], 3rd ed., Chin. Environ. Sci. Publ. House, Beijing, China.

Nesbitt, H. W., and G. M. Young (1982), Early Proterozoic climate and plate motions inferred from major element chemistry of lutites, *Nature*, *299*, 715–717, doi:10.1038/299715a0.

Oldfield, F., and L. Yu (1994), The influence of particle size variations on the magnetic properties of sediments from the north-eastern Irish Sea, *Sedimentology*, *41*(6), 1093–1108, doi:10.1111/j.1365-3091.1994.tb01443.x.

Oldfield, F., B. A. Maher, J. Donoghue, and J. Pierce (1985), Particle-size related, mineral magnetic source sediment linkages in the Rhode River catchment, Marylands, USA, *J. Geol. Soc. London*, *142*(6), 1035–1046, doi:10.1144/gsjgs.142.6.1035.

Oldfield, F., Q. Z. Hao, J. Bloemendal, Z. Gibbs-Eggar, S. Patil, and Z. T. Guo (2009), Links between bulk sediment particle size and magnetic grain-size: General observations and implications for Chinese loess studies, *Sedimentology*, *56*(7), 2091–2106, doi:10.1111/j.1365-3091.2009.01071.x.

Ouyang, T., C. Tian, Z. Zhu, Y. Qiu, E. Appel, and S. Fu (2014), Magnetic characteristics and its environmental implications of core YSJD-86GC sediments from the southern South China Sea, *Chin. Sci. Bull.*, *59*(25), 3176–3187, doi:10.1007/s11434-014-0438-8.

Rahman, R., and A. J. Plater (2014), Particle-size evidence of estuary evolution: A rapid and diagnostic tool for determining the nature of recent saltmarsh accretion, *Geomorphology*, *213*, 139–152, doi:10.1016/j.geomorph.2014.01.004.

Robinson, S. G., J. T. S. Sahota, and F. Oldfield (2000), Early diagenesis in North Atlantic abyssal plain sediments characterized by rock-magnetic and geochemical indices, *Mar. Geol.*, *163*(1–4), 77–107, doi:10.1016/S0025-3227(99)00108-5.

Rowan, C. J., A. P. Roberts, and T. Broadbent (2009), Reductive diagenesis, magnetite dissolution, greigite growth and paleomagnetic smoothing in marine sediments: A new view, *Earth Planet. Sci. Lett.*, *277*, 223–235, doi:10.1016/j.epsl.2008.10.016.

Ru, R. K. (2000), *Analytic Methods of Soil and Agrochemistry* [in Chinese], China Agric. Press, Beijing, China.

Shao, J., S. Yang, and C. Li (2012), Chemical indices (CIA and WIP) as proxies for integrated chemical weathering in China: Inferences from analysis of fluvial sediments, *Sediment. Geol.*, *265*, 110–120, doi:10.1016/j.sedgeo.2012.03.020.

Suganuma, Y., T. Yamazaki, and T. Kanamatsu (2009), South Asian monsoon variability during the past 800 kyr revealed by rock magnetic proxies, *Quat. Sci. Rev.*, *28*(9–10), 926–938, doi:10.1016/j.quascirev.2008.12.014.

Thompson, R., and F. Oldfield (1986), *Environmental Magnetism*, Allen and Unwin, London, U. K.

van den Bergh, G. D., T. C. E. van Weering, J. F. Boels, D. M. Duc, and M. T. Nhuan (2007), Acoustical facies analysis at the Ba Lat delta front (Red River Delta, North Vietnam), *J. Asian Earth Sci.*, *29*(4), 532–544, doi:10.1016/j.jseaes.2006.03.005.

Vinh, V. D., S. Ouillon, T. D. Thanh, and L. V. Chu (2014), Impact of the Hoa Binh dam (Vietnam) on water and sediment budgets in the Red River basin and delta, *Hydrol. Earth Syst. Sci.*, *18*(10), 3987–4005, doi:10.5194/hess-18-3987-2014.

Walden, J., F. Oldfield, and J. Smith (1999), *Environmental Magnetism: A Practical Guide*, Technical Guide No. 6, Quat. Res. Assoc., London, U. K.

Wan, S., et al. (2015), Human impact overwhelms long-term climate control of weathering and erosion in southwest China, *Geology*, *43*(5), 439–442, doi:10.1130/G36570.1.

Wang, S. P., Y. X. Li, S. Y. Fu, R. Xiang, and J. F. Chen (2014), Environmental changes as recorded by mineral magnetic properties of sediments from the core GHE24L, South China Sea [in Chinese], *Quat. Sci.*, *34*(3), 516–527, doi:10.3969/j.issn.1001-7410.2014.03.06.

Yamazaki, T. (2009), Environmental magnetism of Pleistocene sediments in the North Pacific and Ontong-Java Plateau: Temporal variations of detrital and biogenic components, *Geochem. Geophys. Geosyst.*, *10*, Q07Z04, doi:10.1029/2009GC002413.

Yamazaki, T., and M. Ikehara (2012), Origin of magnetic mineral concentration variation in the Southern Ocean, *Paleoceanography*, *27*, PA2206, doi:10.1029/2011PA002271.

Young, G. M., and H. W. Nesbitt (1998), Processes controlling the distribution of Ti and Al in weathering profiles, siliciclastic sediments and sedimentary rocks, *J. Sediment. Res.*, *68*(3), 448–455, doi:10.2110/jsr.68.448.

Zhang, W. G., and L. Z. Yu (2003), Magnetic properties of tidal flat sediments of the Yangtze Estuary and its relationship with particle size, *Sci. China, Ser. D*, *46*, 954–966, doi:10.1007/BF02991341.